

Silicon-on-insulator shortwave infrared wavelength meter with integrated photodiodes for on-chip laser monitoring

M. Muneeb,^{1,2,3,*} A. Ruocco,¹ A. Malik,^{1,2} S. Pathak,^{1,4} E. Ryckeboer,^{1,2} D. Sanchez,^{1,2} L. Cerutti,^{5,6} J.B. Rodriguez,^{5,6} E. Tournié,^{5,6} W. Bogaerts,^{1,7} M.K. Smit,³ and G. Roelkens^{1,2,3}

¹Photonics Research Group, Department of Information Technology, Ghent University - IMEC, Sint-Pietersnieuwstraat 41, 9000 Ghent, Belgium

²Center for Nano- and Biophotonics (NB-Photonics), Ghent University, Belgium

³COBRA Research Institute, Eindhoven University of Technology, P.O. Box 513, Eindhoven 5600 MB, The Netherlands

⁴Currently with University of California Davis, Dept. of Electrical and Computer Engineering, Davis, CA 95616, USA

⁵Université de Montpellier, IES, UMR 5214, F-34000 Montpellier, France

⁶CNRS, IES, UMR 5214, F-34000 Montpellier, France

⁷Luçeda Photonics, Dendermonde, Belgium

*muhammad.muneeb@intec.ugent.be

Abstract: This paper demonstrates a very compact wavelength meter for on-chip laser monitoring in the shortwave infrared wavelength range based on an optimized arrayed waveguide grating (AWG) filter with an integrated photodiode array. The AWG response is designed to obtain large nearest neighbor crosstalk (i.e. large overlap) between output channels, which allows accurately measuring the wavelength of a laser under test using the centroid detection technique. The passive AWG is fabricated on a 220 nm silicon-on-insulator (SOI) platform and is combined with GaInAsSb-based photodiodes. The photodiodes are heterogeneously integrated on the output grating couplers of the AWG using DVS-BCB adhesive bonding. The complete device with AWG and detectors has a footprint of only 2 mm² while the measured accuracy and resolution of the detected wavelength is better than 20pm.

©2014 Optical Society of America

OCIS codes: (130.0130) Integrated optics; (040.3060) Infrared; (040.0040) Detectors.

References and links

1. E. Ryckeboer, A. Gassenq, M. Muneeb, N. Hattasan, S. Pathak, L. Cerutti, J. B. Rodriguez, E. Tournié, W. Bogaerts, R. Baets, and G. Roelkens, "Silicon-on-insulator spectrometers with integrated GaInAsSb photodiodes for wide-band spectroscopy from 1510 to 2300 nm," *Opt. Express* **21**(5), 6101–6108 (2013).
2. R. N. John, I. Read, and W. N. MacPherson, "Design considerations for a fibre Bragg grating interrogation system utilizing an arrayed waveguide grating for dynamic strain measurement," *Meas. Sci. Technol.* **24**(7), 075203 (2013).
3. R. Yu, R. Proietti, J. Kurumida, A. Karalar, B. Guan, and S. J. B. Yoo, "Rapid high-precision in situ wavelength calibration for tunable lasers using an athermal AWG and a PD array," *IEEE Photon. Technol. Lett.* **24**(1), 70–72 (2012).
4. G. Roelkens, U. D. Dave, A. Gassenq, N. Hattasan, C. Hu, B. Kuyken, F. Leo, A. Malik, M. Muneeb, E. M. P. Ryckeboer, D. Sanchez, S. Uvin, Z. Hens, R. Baets, Y. Shimura, F. Gencarelli, B. Vincent, R. Loo, J. V. Campenhout, L. Cerutti, J. B. Rodriguez, E. Tournié, X. Chen, and M. Nedeljkovic, "Silicon-based photonic integration beyond the telecommunication wavelength range," *IEEE J. Sel. Top. Quantum Electron.* **20**(4), 8201511 (2014).
5. M. K. Smit and C. Van Dam, "PHASAR-based WDM-devices: principles, design and applications," *IEEE J. Sel. Top. Quantum Electron.* **2**(2), 236–250 (1996).
6. W. Bogaerts, P. Dumon, D. V. Thourhout, D. Taillaert, P. Jaenen, J. Wouters, S. Beckx, V. Wiaux, and R. Baets, "Compact wavelength selective functions in silicon-on-insulator photonic wires," *IEEE J. Sel. Top. Quantum Electron.* **12**(6), 1394–1401 (2006).
7. <http://www.epixfab.eu/>

1. Introduction

Recently, the interest in the shortwave infrared wavelength region (2 – 3 μm) has increased a lot for next generation communication systems as well as for spectroscopic applications due to the strong absorption of many molecules in this wavelength range [1]. Integrated tunable lasers are an important component for such systems. To tune and control these lasers accurately an on-chip integrated wavelength meter is desirable, which can give feedback to the laser driving circuitry. In this paper we demonstrate such a wavelength meter based on an AWG whose response is tailored to intentionally increase nearest neighbor crosstalk (NXT, defined as the power level at which two neighboring channels cross each other). By using a centroid detection technique the absolute wavelength of the laser is detected with much higher accuracy than the channel spacing of the AWG itself. While a similar concept has been implemented for a fiber Bragg grating interrogator [2] and for laser tuning [3], this is the first implementation for the shortwave infrared (SWIR) wavelength range. At the same time we present a fully integrated device, having an AWG and a photodiode array integrated on the same chip. The implementation of the wavelength meter on a silicon photonics platform can potentially lead to low-cost volume manufacturing. Also, a similar GaInAsSb-based material system as used for the photodiode array can be used to integrate the laser itself [4].

2. Working principle

The key component of the wavelength meter being presented here is an AWG. A conventional AWG is usually used as wavelength demultiplexer which can separate different wavelengths. When used for such purpose low nearest neighbor cross-talk (NXT) is required. However to use an AWG as a wavelength meter we intentionally increase NXT such that an input laser line produces a measurable output over several AWG channels. Then by using the center of gravity Eq. (1) we can estimate the wavelength of the laser line.

$$\text{CoG} = \frac{\sum_i P_{CH_i} \cdot i}{\sum_i P_{CH_i}} \quad (1)$$

Here i is the AWG channel number index, P_{CH_i} is the measured response of the i_{th} AWG channel and CoG is the center of gravity. The CoG value corresponds to the input wavelength of the laser under test. Figure 1 shows this working principle in graphical form.

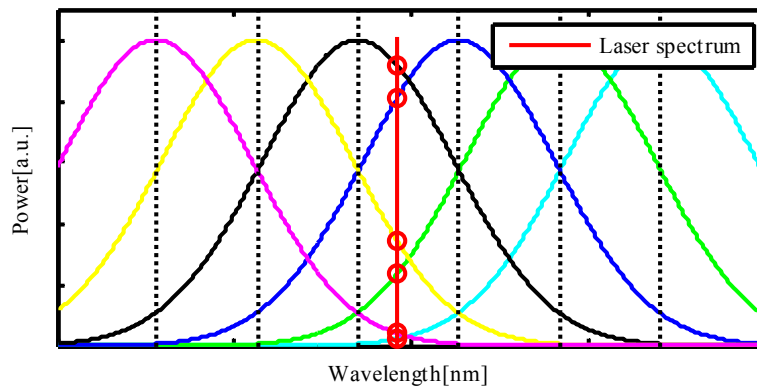


Fig. 1. Working principle of a wavelength meter where an input laser line produces measurable outputs over few channels and the laser wavelength is estimated by using the center of gravity Eq. (1).

3. Design

A conventional AWG (de)multiplexer design [5] consists of two free propagation regions (FPR) which provide the (de)focusing functionality. These two FPRs are connected together by an array of waveguides having a constant incremental optical path difference. Input light diffracts into the first FPR through an input aperture and is coupled to an array of delay waveguides. After passing through the second FPR different input wavelengths are focused on a number of output apertures. In a conventional AWG, both input and output apertures have the same cross-section which ensures maximal overlap of the optical fields and hence low insertion losses. Also a steep roll off (hence small NXT, a desired characteristic in a demultiplexer) of the channel response is achieved for small wavelength deviations with respect to the corresponding center wavelength of the channel.

For our application we use a wider input aperture compared to the output aperture in order to achieve large NXT. As a result a large image is formed on the image focal plane, which overlaps with a number of output apertures and hence provides the required large NXT. But this large NXT comes at an expense of reduced peak channel transmission as the input signal is now divided into a number of overlapping channels.

To find out the effect of NXT on the performance of the proposed wavelength meter, Fig. 2 shows a simulation example where the AWG output channel response is assumed to be Gaussian, the output channel wavelength spacing is fixed at 3 nm and ten channels are used to calculate CoG. The NXT is varied in order to assess its influence on the performance of the wavelength meter. We can see that when the NXT value is smallest i.e. when only two neighboring channels give a reasonable response, the slope of the curve (which represents the sensitivity of the wavelength meter to a change in the input wavelength) varies as function of input wavelength. When the NXT is increased the curve becomes more and more linear which is a desirable characteristic to have the same sensitivity over the complete wavelength range of operation. The inset of Fig. 2 shows the norm of the residuals for a linear fit to the CoG curve as a function of NXT.

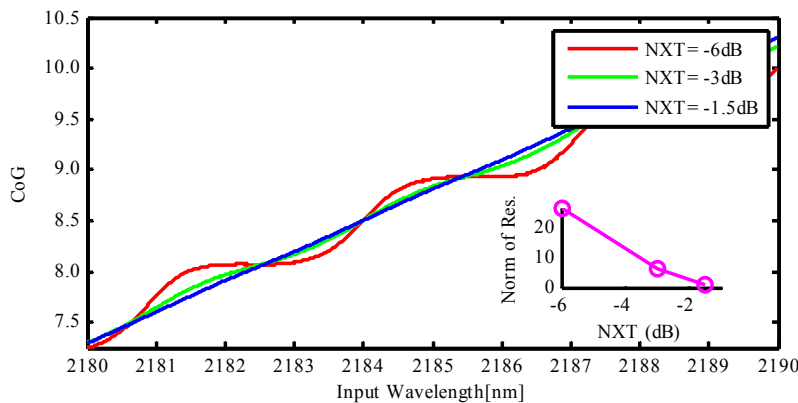


Fig. 2. Effect of NXT on the linearity of the CoG curve. The inset shows the norm of the residuals for a linear fit.

From these simulations in order to achieve NXT value of -1.5dB , we have chosen input and output apertures of $5\ \mu\text{m}$ and $1.5\ \mu\text{m}$ respectively, which is a tradeoff between the linearity of the CoG curve and peak channel transmission. To reduce the phase errors in the arrayed waveguide structure due to waveguide width variations in fabrication we used expanded waveguides in long straight sections of the AWG delay lines [6]. Single mode 750nm wide input and output access waveguides are connected to $20\ \mu\text{m}$ wide waveguides through linear tapers. Vertical grating couplers ($1.51\ \mu\text{m}$ period and 65% fill factor of the 220nm deep etched slits) are implemented on these wide waveguides which are used for passive characterization of the AWG and later on to integrate the photodiodes on the output

grating couplers. The exit angle of grating couplers is around 5 degrees at a wavelength of $2.2\mu\text{m}$. All photonic components (AWG, waveguides and grating couplers) are designed for TE-polarized light and a center wavelength of $2.2\mu\text{m}$. Figure 3 shows a schematic view of designed AWG with important layout parameters.

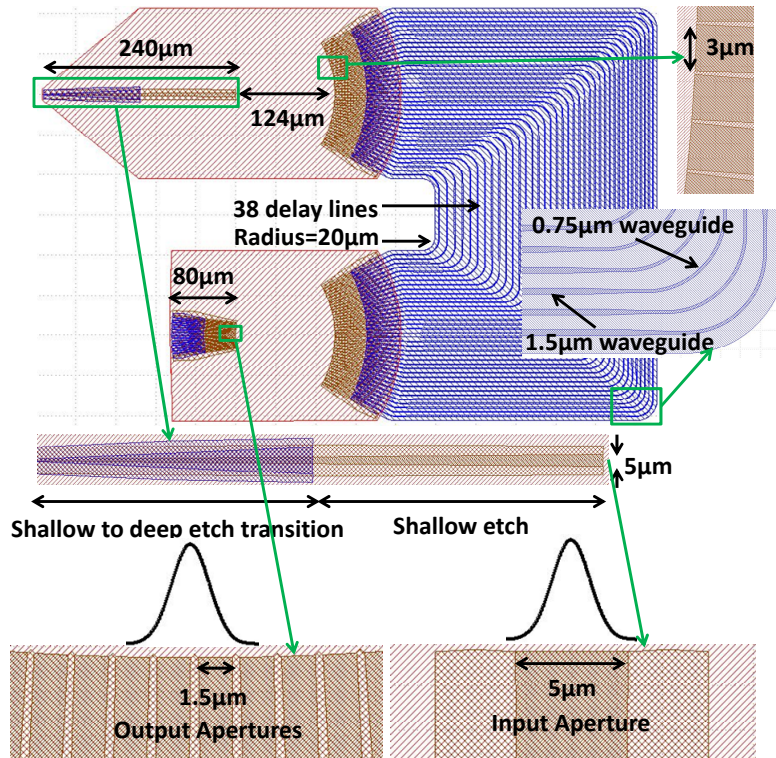


Fig. 3. Schematic view of the designed AWG with layout parameter values. It is also schematically shown that the image formed on the image focal plane overlaps with a number of output apertures, which allows the accurate detection of the center of gravity of the image (and hence its wavelength).

4. Fabrication

4.1 Passive waveguide circuit

The multiproject wafer run (MPW) fabrication service offered by imec, Belgium through ePIXfab [7] was used to fabricate the passive photonic waveguide circuit. Fabrication is carried out in a CMOS pilot line on 200mm SOI wafers, comprising of a 220nm thick silicon layer on a 2 μm buried oxide layer. Two etching steps of 70nm (shallow etch) as well as 220nm (deep etch) were available in this MPW run. The shallow etch is used to define the star couplers of the AWG followed by a deep etch to define deep to shallow transitions in star couplers, access waveguides, AWG delay lines and vertical grating couplers. Finally, SiO_2 is deposited and planarized which acts as top cladding. The final thickness of the top cladding after planarization is 1.25 μm on top of the waveguides. Planarization of the top cladding is important for the bonding of III-V material during the post-processing of the chip to fabricate the photodiode array. Figure 4 shows a microscope image of the fabricated device.

4.2 Photodiodes

The shortwave infrared photodiode array was heterogeneously integrated on top of the silicon waveguide circuit. To fabricate photodiodes on top of the output grating couplers we used a GaSb-based III-V epistack grown by solid-source Molecular Beam Epitaxy (MBE). Be and

Te are used as p- and n-type dopants. The substrate was (100) oriented n-type GaSb. First the substrate is de-oxidized at 550°C, and then a GaSb buffer layer is grown at 500°C followed by 0.5μm of InAs_{0.91}Sb_{0.09}. This layer will be used as etch stop layer while removing the GaSb substrate during the integration process. After the etch stop layer, the p-i-n junction is grown. The p-type zone consists of 50 nm of GaSb and 50nm Ga_{0.79}In_{0.21}As_{0.19}Sb_{0.81} (both doped 10¹⁸ cm⁻³). An un-intentionally doped 500nm thick Ga_{0.79}In_{0.21}As_{0.19}Sb_{0.81} layer is used as intrinsic absorption zone. Finally a 50nm thick Ga_{0.79}In_{0.21}As_{0.19}Sb_{0.81} and 150nm InAs_{0.91}Sb_{0.09} layer is grown as the n-type region (doped 10¹⁸ cm⁻³). This epistack has a bandgap wavelength of 2.65 μm at room temperature.

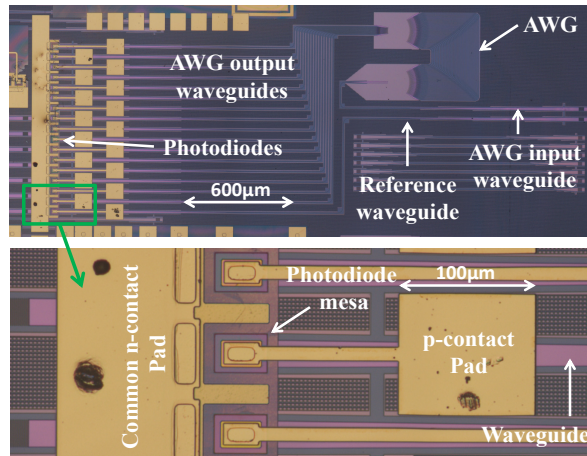


Fig. 4. Microscope image of the complete fabricated device with a zoom-in on the integrated photodiode.

After cleaning the SOI chip containing the passive waveguide circuit a DVS-BCB:mesitylene solution is applied by spin-coating. By choosing the volume ratio of DVS-BCB to mesitylene and spin speed we can control the DVS-BCB thickness. We used a 40% DVS-BCB by volume solution to achieve a film thickness of around 300nm. After spin coating the chip is pre-baked on a hotplate at 150°C for 5 minutes to evaporate residual mesitylene. The III-V die (~4mmx4mm) is then manually attached to the chip, epitaxial layers down and the sample is clamped in the bonding machine (Karl Suss Microtech CB6L) fixture. The fixture is loaded into the machine chamber where a vacuum (4×10^{-4} mbar) is created and the sample is baked at 250°C under moderate bonding pressure during 1 hr. After the bonding process, the 500μm thick GaSb substrate is mechanically grinded down to ~75μm. The remaining GaSb substrate is removed by wet etching with a HF/CrO₃ [8] solution, until the etch stop layer (InAs_{0.91}Sb_{0.09}) is reached. The etch stop layer is removed using a citric acid:H₂O₂ (2:1 v/v) solution. The photodiode mesa (30μm x 40μm) is formed, lithographically aligned to the underlying output grating couplers, by wet etching (citric acid:H₂O₂:H₃PO₄:H₂O 55:5:3:220 v/v). Ti(2nm)/Pt(35nm) and Au(100nm) are deposited using an e-beam evaporation system for both p and n-type contacts. To passivate the photodiodes BCB is spincoated on the sample and cured at 250°C for 1 hr. Then to access the top and bottom metallization, BCB vias are dry etched in a reactive ion etcher. The etching gas mixture is SF₆/O₂ (5:50sccm) and the etch rate of BCB is 280 nm/min. Finally, the process ends with the deposition of Ti(40nm)/Au(500nm) for the final contact pads. A schematic cross-section of the photodiode is shown in Fig. 5 together with the SEM cross-section of a fabricated photodiode.

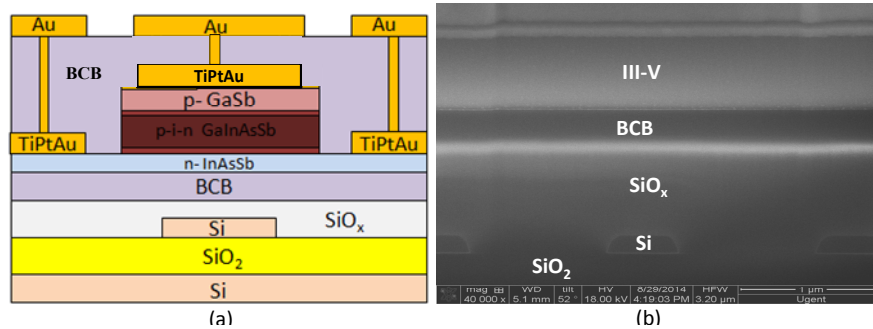


Fig. 5. (a) Schematic cross-section view of the photodiode showing the III-V layer stack used. (b) SEM cross-section of the fabricated photodiode.

5. Characterization

To characterize the fabricated wavelength meter we used a measurement setup schematically shown in Fig. 6. SWIR laser light from a tunable $\text{Cr}^{2+}:\text{ZnSe}$ laser from IPG Photonics is coupled to single mode fiber and fed to a 99/1% splitter. Light from the 1% arm is then connected to an optical spectrum analyzer (Yokogawa AQ6375) and light from the 99% arm is coupled to the input grating coupler of the fabricated chip injecting TE-polarized light into the chip. The chip is mounted on a Peltier stage whose temperature is controlled within $\pm 0.1^\circ\text{C}$. A bias voltage is applied to the photodiodes through electrical probes connected to a Keithley 2400. The same system is used to measure the generated photocurrent by the photodiodes.

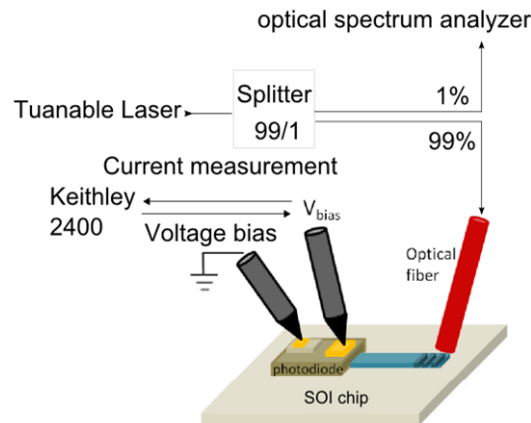


Fig. 6. Schematic of measurement setup used for characterization.

The average dark current of the photodiodes at a bias voltage of -1V and -10mV is $15\mu\text{A}$ and $0.5\mu\text{A}$ respectively. By measuring a reference waveguide on the same chip without an integrated photodiode we estimated the peak fiber coupling efficiency of the grating coupler to be -8 dB per grating coupler (80nm 3dB bandwidth). By using this coupling efficiency we estimated the optical power in the waveguide. Then by measuring another reference waveguide with a photodiode integrated on the output grating coupler we estimated the on-chip photodiode responsivity to be 0.51 A/W .

The transmission response of the AWG channels was measured by sweeping the laser wavelength from 2185nm to 2225nm with steps of 0.5nm and recording the photocurrent for each wavelength step. This process was repeated for 10 AWG channels. Figure 7 shows the measured response of the AWG channels. By normalizing the AWG response with a reference waveguide we found that the AWG has about 4dB insertion loss. All AWG

channels show reasonable cross-talk levels of -18dB and an NXT of about -1.5dB , which is in line with the simulations presented in section 3.

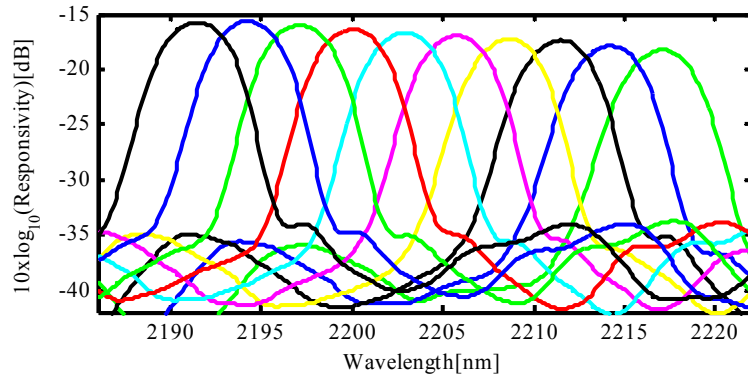


Fig. 7. Response of the AWG with integrated photodiodes.

Using Eq. (1), the CoG is calculated for each wavelength step of the measured transmission response of the AWG. This calculated CoG as function of wavelength is plotted in Fig. 8. This curve is named the calibration curve. If some unknown wavelength is sent to the input of the AWG we can calculate the CoG using the photo-response of all 10 photodiodes connected to the AWG. Using the calibration curve the unknown wavelength can be estimated.

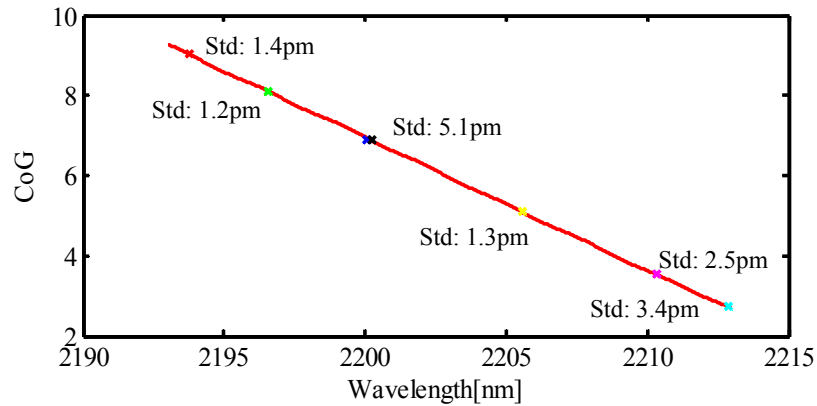


Fig. 8. Calibration curve with 'x' marks showing the tested wavelengths and standard deviation of their detection error.

A number of wavelengths in the operating wavelength range of the wavelength meter were tested. At least 50 measurements were performed for each wavelength. In Fig. 8 the 'x' marks show the mean calculated CoG. The standard deviation of the detection error for each tested wavelength is also indicated. The detection error is defined as the difference between the detected wavelength (using the calibration curve) and the true wavelength (measured using an optical spectrum analyzer).

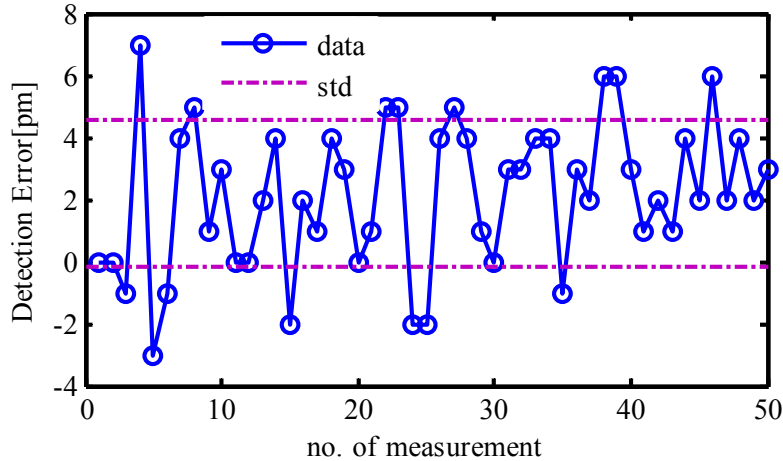


Fig. 9. Detection error for a test wavelength of 2200.20nm based on 50 measurements.

All tested wavelengths show a detection error of less than 20pm with a standard deviation of less than 6pm. Figure 9 shows the detection error for one tested wavelength (2200.20nm) when measurements are repeated 50 times. The wavelength meter accuracy is limited by the combined effect of different noise sources (e.g. photodiode noise, mechanical vibration of the incoupling fiber and small temperature variations). Probably by measuring all photodiodes in parallel instead of serial will reduce the effect of some of these noise sources, which can further improve the detection accuracy. Figure 10 shows that we can also use our wavelength meter to detect mode hopping of a laser. In this experiment a set of 50 measurements is carried out at one wavelength (i.e. 2200.20nm) after which the laser wavelength is increased by 20pm (i.e. 2200.24nm) and another set of 50 measurements is carried out. Figure 10 shows that we can detect this small wavelength change with our wavelength meter. In a real laser mode-hopping case one can monitor the detected wavelength as a function of time and if the variation in the detected wavelength is more than a typical standard deviation (i.e. less than 10pm) of our wavelength meter, then a mode-hop is identified.

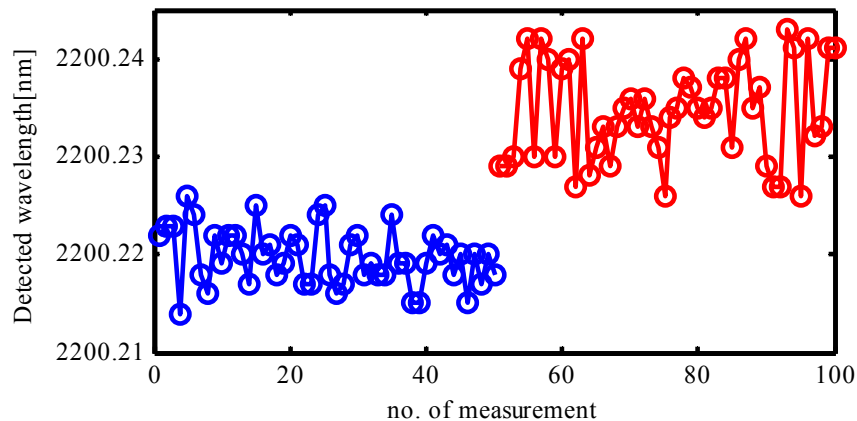


Fig. 10. Detection of two nearby wavelengths (2200.22nm and 2200.24nm).

6. Conclusion

We have demonstrated a compact wavelength meter for on-chip laser monitoring. We showed that by using a relatively large channel spacing of 3nm in an optimized AWG with large NXT, the wavelength detection accuracy for a narrow linewidth source can be increased by

more than a factor of 150. This results in a device with better than 20pm wavelength resolution on a 2mm² footprint. The fabrication process is scalable both in terms of the SOI waveguide circuit fabrication as well as photodiode integration.

Acknowledgments

This work was carried out in the framework of the FP7-ERC project MIRACLE and STW project LWAVETECH.